Effect of oxalic acid on the selective flotation separation of Pb-activated sphalerite from galena

Doaa Ashraf Eladl
Graduate School of Engineering, Faculty of Engineering, Kyushu University

Gde Pandhe Wisnu Suyantara
Department of Earth Resources Engineering, Faculty of Engineering, Kyushu University

Miki, Hajime
Department of Earth Resources Engineering, Faculty of Engineering, Kyushu University

Akbarshokh Ulmaszoda
Graduate School of Engineering, Faculty of Engineering, Kyushu University

他

出版情報：Advanced Powder Technology. 36 (4), pp.104818-, 2025-04. 粉体工学会
バージョン：

Advanced Powder Technology 36 (2025) 104818

Contents lists available at ScienceDirect

Advanced Powder Technology

journal homepage: www.elsevier.com/locate/apt

Original Research Paper

Effect of oxalic acid on the selective flotation separation of Pb-activated sphalerite from galena

Doaa Ashraf Eladl [a], Gde Pandhe Wisnu Suyantara [b,c,*], Hajime Miki [b], Akbarshokh Ulmaszoda [a], Naoko Okibe [b,*]

[a] Graduate School of Engineering, Faculty of Engineering, Kyushu University, Fukuoka, Japan
[b] Department of Earth Resources Engineering, Faculty of Engineering, Kyushu University, Fukuoka, Japan
[c] School of Innovation, Science, and Interdisciplinary, Kyushu University, Fukuoka, Japan

ARTICLE INFO

Article history:
Received 22 November 2024
Received in revised form 31 January 2025
Accepted 7 February 2025
Available online 13 February 2025

Keywords:
Sphalerite activation
Galena
Pb-Zn selective flotation
Oxalic acid

ABSTRACT

The separation of sphalerite (ZnS) and galena (PbS) is challenging owing to activation of the sphalerite surface by unavoidable metal ions, such as lead ions (Pb^{2+}) released from lead-containing minerals. In this study, oxalic acid (OA) was applied for the first time as an environmentally friendly reagent to deactivate the sphalerite surface in lead–zinc (Pb-Zn) flotation separation. Micro-flotation experiments showed that OA, at a concentration of 0.56 mM, significantly reduced sphalerite recovery. Single-mineral flotation tests demonstrated that sphalerite recovery decreased to 20 %, while galena recovery remained at 58.7 % after OA treatment. Further flotation tests on an artificial mixture of sphalerite and galena confirmed effective separation with OA treatment under mildly alkaline conditions, achieving recoveries of 83 % for galena and 17 % for sphalerite. Infrared spectroscopy and X-ray photoelectron spectroscopy analyses showed that OA removes Pb^{2+} ions from the surface of sphalerite by forming lead oxalate (Pb (II)-Ox) precipitates, which detach from the sphalerite surface, effectively cleaning it. This detachment prevents the adsorption of potassium amyl xanthate (PAX) by forming a dispersed lead oxalate-amyl xanthate (PbOx-AX) complex, which exposes the hydrophilic sphalerite surface and leads to its depression. In contrast, this interaction had a minimal impact on the floatability of galena.

1. Introduction

Sulfide minerals are among the most varied and abundant types of minerals. They exhibit a broad range of physical, chemical, and structural properties and are considered a rich source of important metals such as copper (Cu), lead (Pb), and zinc (Zn) [1,2]. Sphalerite (ZnS) and galena (PbS) are the primary sources for Zn and Pb extraction. They often coexist in sulfide ores and are typically separated by selective flotation, with galena being recovered first, followed by sphalerite [3–6]. Generally, galena exhibits excellent natural floatability due to its crystal structure [7]. Thiol collectors, such as xanthates, are commonly applied in the flotation of sulfide minerals, and they have a high affinity to adsorb on the galena surface [8–10]. In contrast, sphalerite has low reactivity with most thiol collectors due to the high solubility of zinc xanthate [11,12].

However, in lead–zinc (Pb-Zn) sulfide ores, sphalerite recovery increases along with galena, making Pb-Zn separation more challenging [13]. This is due to sphalerite activation by lead species, which occurs during multiple stages, including mining, grinding [4], and the recycling of plant water [11]. It has been reported that sphalerite activation mainly results from the natural dissolution of associated Pb minerals, such as galena and anglesite ($PbSO_4$), which release lead ions (Pb^{2+}). These Pb^{2+} ions activate sphalerite through an ion exchange mechanism, replacing zinc ions (Zn^{2+}) with Pb^{2+} ions [4]. This process leads to the formation of lead sulfide (PbS) precipitates on the sphalerite surface, increasing its hydrophobicity and significantly affecting Pb-Zn separation efficiency, ultimately reducing the mineral concentrate grade [11,14]. Therefore, to achieve efficient Pb-Zn separation, it is necessary to use selective reagents to inhibit Pb-activated sphalerite flotation without affecting galena.

Several studies have been conducted on sphalerite deactivation by applying different reagents, known as depressants, to separate sphalerite from galena through flotation [3,13,14]. Inorganic depressants are widely used in industrial Pb-Zn flotation processes

* Corresponding authors.
E-mail addresses: pandhe@mine.kyushu-u.ac.jp (G.P. Wisnu Suyantara), okibe@mine.kyushu-u.ac.jp (N. Okibe).

https://doi.org/10.1016/j.apt.2025.104818

for sphalerite depression. For example, cyanide deactivates the sphalerite surface by reacting with activator species, such as copper ions (Cu^{2+}), to form metal cyanide complexes [15]. El-Shall et al. [16] investigated the deactivation mechanism of zinc sulfate in sphalerite depression and suggested that Pb^{2+} ions on the surface of activated sphalerite are replaced by Zn^{2+} ions. Other inorganic depressants, such as potassium dichromate ($K_2Cr_2O_7$) and sulfur oxides—including sulfur dioxide (SO_2), sodium sulfite (Na_2SO_3), and sodium bisulfite ($NaHSO_3$)— have also been studied [17]. However, these inorganic depressants have several drawbacks, including low selectivity, the requirement for high alkaline conditions, high toxicity, high dosage, and poor biodegradability, which make their disposal challenging and environmentally hazardous [18]. Consequently, the application of inorganic depressants in flotation is restricted.

To maintain sustainable mineral processing and reduce environmental pollution, organic depressants have gained increasing attention in recent years due to their sustainability, abundant resources. Currently, the organic depressants used in Pb-Zn flotation are mainly organic polymers rich in functional groups, such as carboxyl (–COOH), hydroxyl (–OH), and benzene rings [19]. Examples include pectin [17], guar gum [20], pullulan [21], chitosan [22], and dextrin [23]. The mechanism of these organic depressants involves the selective binding of functional groups to the sphalerite surface, forming a hydrophilic layer that prevents potassium amyl xanthate (PAX) adsorption while having minimal impact on galena [17,20–23]. Although organic polymers show potential for selectively inhibiting sphalerite in Pb-Zn flotation, they are poorly soluble and challenging to implement on an industrial scale [18]. In addition, these studies did not investigate how these organic depressants interact preferentially with Pb-activated sphalerite, as their inhibition mechanisms primarily focused on a non-activated sphalerite surface.

There have been few published reports on the selective depression of activated sphalerite using environmentally friendly reagents. For example, dextrin deactivates sphalerite by selectively reacting with metal hydroxide species on the sphalerite surface to form metal complexes, thereby reducing its floatability by limiting xanthate collector adsorption [24]. Polyphosphate (PP) has been shown to deactivate the sphalerite surface by removing lead species through a surface-cleaning mechanism, in which PP forms soluble complexes, leading to decreased sphalerite recovery [25]. Aikawa et al. [14] studied the effect of ethylenediaminetetraacetic acid (EDTA) as a pretreatment agent for surface cleaning, which removes lead-soluble compounds, such as anglesite, in combination with zinc sulfate ($ZnSO_4$) to depress lead-activated sphalerite.

Given the scarcity of research in this area, there is a clear need to explore more environmentally friendly depressants. Oxalic acid (OA), a naturally occurring dicarboxylic acid, is classified as a low molecular weight organic acid (LMWOA) and is commercially available in dihydrate form [26,27]. OA can be sustainably synthesized from renewable sources through the fermentation of cheap carbon sources, such as agricultural waste and microorganisms. It is readily biodegradable and is not considered a significant environmental pollutant [28]. In aqueous solutions, OA exists in multiple oxalate ion species ($H_2C_2O_4$, $H_2C_2O_4^-$, and $C_2O_4^{2-}$) depending on the pH of the system [29]. Moreover, oxalate ions exhibit a strong ability to bind metal cations through chelation [30], making them useful in various metal recovery and hydrometallurgical applications, including the extraction of metals from ores [31,32], lithium-ion battery recycling [33,34], spent catalyst recovery [35], and the treatment of industrial waste streams [36–39].

In the froth flotation process, OA is used as an environmentally friendly depressant for the separation of silicate minerals, such as olivine and titanaugite. It interacts with metal cations on mineral surfaces, inhibiting collector adsorption [29]. In contrast, OA acts as an activator in pyrite flotation, reacting with hydrophilic species on the mineral surface to promote flotation recovery [40,41]. Suyantara et al. [42] investigated the role of OA in pyrite–chalcopyrite separation and found that OA inhibited copper activation of pyrite by forming copper oxalate, which prevented PAX adsorption. However, in the Pb-Zn flotation system, the use of OA as a depressant has not been previously reported.

In this study, OA was selected due to its unique properties and previous applications in flotation systems, particularly its ability to form oxalate-metal complexes. Oxalate ($C_2O_4^{2-}$) ions are known to form complexes with lead (Pb^{2+}) in alkaline system [43], suggesting their potential application in Pb-Zn separation. Therefore, this study investigates the effectiveness of OA as a novel, environmentally friendly depressant for preventing Pb-activated sphalerite flotation. Furthermore, the selective separation of Pb-activated sphalerite from galena using OA is evaluated. The flotation performance of Pb-activated sphalerite and galena is assessed using both pure and mixed minerals. Additionally, the effect of OA on the surface properties of Pb-activated sphalerite and galena is analyzed using Fourier transform infrared spectroscopy (FTIR) and X-ray photoelectron spectroscopy (XPS).

2. Materials and Methods

2.1. Materials

Sphalerite (Akita Prefecture, Japan) and galena (Yamagata Prefecture, Japan) were purchased from Komuro Minerals (Tokyo). The X-ray diffraction (XRD) patterns of both minerals are shown in Fig. 1. Chemical analysis by X-ray fluorescence (XRF) indicated that sphalerite consists of 66.3 % Zn, 30.1 % S, and 1.3 % Fe, and galena consists of 80.7 % Pb and 12.1 % S. After being crushed with an agate mortar and pestle, samples with particle sizes below 106 μm were used for micro-flotation experiments. The particle size of the samples for surface analysis using FTIR and XPS was less than 38 μm. Analytical-grade oxalic acid ($(COOH)_2$; OA), lead nitrate ($Pb(NO_3)_2$), potassium amyl xanthate ($CH_3(CH_2)_4OCS_2K$; PAX), sodium hydroxide (NaOH), hydrochloric acid (HCl), and methyl pentanol ($C_6H_{13}OH$; MIBC) were purchased from Fujifilm Wako Pure Chemical Corporation (Tokyo, Japan).

2.2. Micro-flotation experiments

Micro-flotation experiments were conducted to study the floatability of both pure and mixed sphalerite and galena under various treatment conditions. In the single flotation tests, 0.6 g of pure mineral samples were dispersed in 180 mL of ultrapure water using a magnetic stirrer, resulting in a pulp density of 0.33 %. The mineral suspension was subsequently treated with $Pb(NO_3)_2$ (0.12 mM) to simulate the Pb-activation of sphalerite. After this treatment, various concentrations of OA (0–0.56 mM) were added to evaluate its effect on sphalerite flotation. PAX (30 g/t) was then introduced as a collector, followed by the addition of MIBC (0.22 μM) as a frothing agent. The treatment time for each reagent is shown in Fig. 2. The pH of the suspension was adjusted to the desired range (6–11) using NaOH and HCl. Micro-flotation tests were performed using a modified Partridge-Smith column flotation setup [44].

Mixed sphalerite-galena flotation separation tests were conducted to verify the selective separation performance of oxalic acid. A suspension of mixed minerals was prepared by mixing 0.3 g of sphalerite and 0.3 g of galena in 180 mL of ultrapure water (1:1 mass ratio), resulting in a final pulp density of 0.33 %. The mixed flotation treatments followed the same procedure as the single mineral flotation, with an additional evaluation of PAX concentrations at 30 g/t and 120 g/t. The procedural schematic

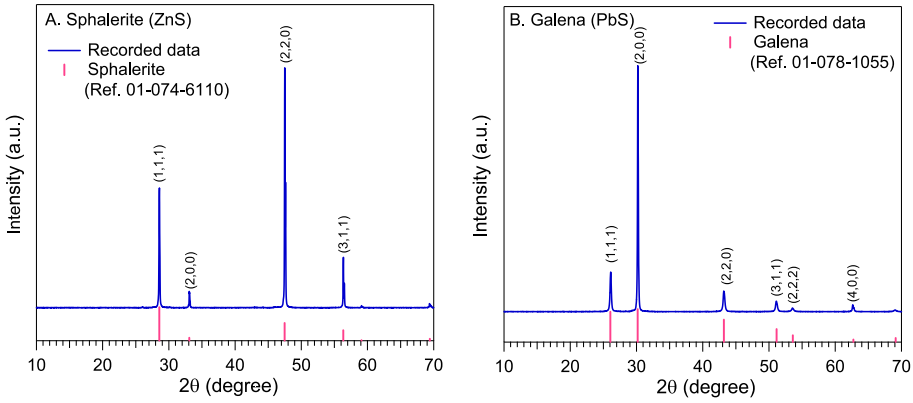

Fig. 1. X-ray diffraction patterns of (A) sphalerite and (B) galena.

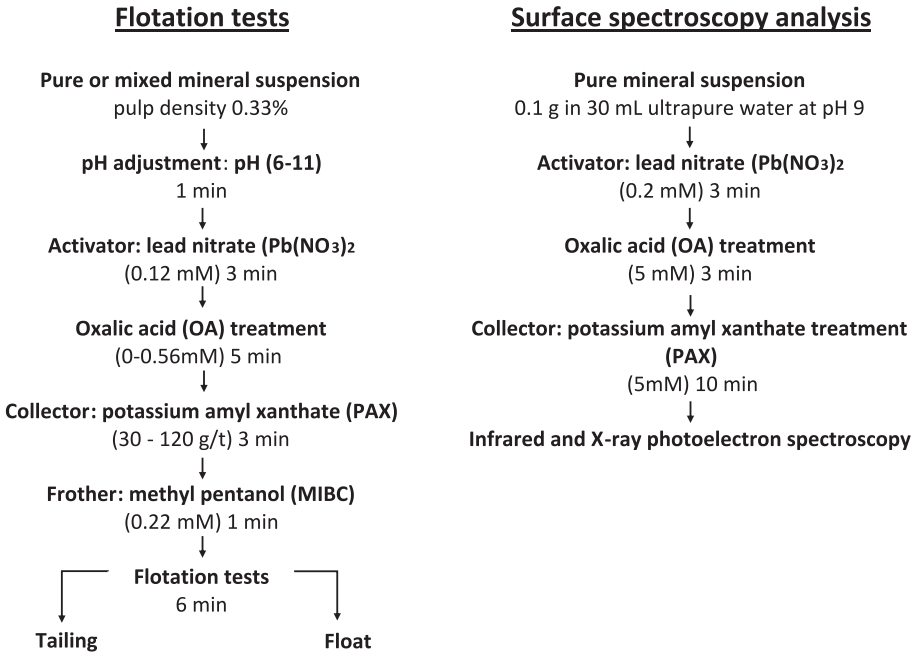

Fig. 2. Schematic process for mineral treatments in flotation tests and surface spectroscopy analysis.

for column flotation has been previously reported [45–47]. Nitrogen gas was introduced at a flow rate of 20 mL/min. The froth was collected over 6 min, after which the tailing and froth fractions were filtered and dried in an oven (WFO-520, Eyela, Tokyo, Japan) at 60 °C for 24 h. Flotation recovery of each mineral was calculated using Equation (1) [45,48]:

$$\text{Recovery}\,(\%) = \frac{C}{C+T} \times 100\,\% \tag{1}$$

in which C is the mass of the concentrate and T is the mass of the tailings. The flotation recovery was determined by dividing the mass of the concentrate (C) by the total mass of both the concentrate and tailings (C + T). Each experiment was conducted in duplicate, and the average recovery is reported in this study.To assess the efficiency of Pb-Zn separation, Equation (2) was used [45]:

$$\text{Separation efficiency}\,(\%) = \text{Pb recovery}\,(\%) - \text{Zn recovery}\,(\%) \tag{2}$$

2.3. Surface spectroscopy analysis

To further study the effect of OA on the surfaces of sphalerite and galena, FTIR and XPS analyses were conducted under various conditions. A mineral suspension was prepared by mixing 0.1 g of mineral powder with 30 mL of ultrapure water, as illustrated in Fig. 2. The suspension was treated with 0.2 mM $Pb(NO_3)_2$ for 3 min, followed by 5 mM OA for 3 min and then 5 mM PAX for 10 min. The reagent concentrations used for spectroscopy analysis were higher than those in flotation tests to obtain clearer spectra data. After treatment, the mineral suspension was filtered, collected, and dried at room temperature.

To study the interaction between $Pb(NO_3)_2$, OA, and PAX, chemically synthesized lead oxalate (PbC_2O_4; PbOx) was prepared as a reference. This was done by mixing 10 mL of 0.2 M OA with 10 mL of 0.1 M $Pb(NO_3)_2$ at pH 9, resulting in the formation of white precipitates, as shown in Equation (3) [49]:

$$Pb^{2+}{}_{(aq)} + {C_2O_4}^{2-}{}_{(aq)} \rightarrow PbC_2O_{4\,(s)} \tag{3}$$

Similarly, lead amyl xanthate ($CH_3(CH_2)_4OCS_2Pb$; PbAX) was synthesized by mixing 10 mL of 0.1 M $Pb(NO_3)_2$ with 10 mL of 0.2 M

PAX at pH 9, forming yellowish precipitates, as shown in Equation (4) [50]:

$$Pb^{2+}{}_{(aq)} + 2CH_3(CH_2)_4OCS_2{}^{-}{}_{(aq)} \rightarrow Pb(CH_3(CH_2)_4OCS_2)_{2(s)} \quad (4)$$

To investigate the product formed by the reaction of PbOx with PAX, PbOx was first prepared, as described above. Then, 10 mL of 0.2 M PAX was added to the PbOx mixture, resulting in yellowish precipitates of lead oxalate-amyl xanthate ($PbC_2O_4CH_3(CH_2)_4OCS_2$; PbOx-AX). The precipitates were filtered and collected for FTIR and XPS analyses.

FTIR analysis of precipitates and treated minerals was conducted using the attenuated total reflection (ATR) method, with a spectral range of 400–4000 cm^{-1} (FTIR spectrometer 670 Plus, JASCO, Tokyo, Japan). XPS analysis was performed using an AXIS-ULTRA instrument (Shimadzu, Japan) under a vacuum pressure of 10^{-9} Pa. Wide survey and high-resolution spectral scans were performed to determine the chemical states and bonding configurations. Spectra were analyzed using CasaXPS software (Ver. 2.3.16), applying Shirley background corrections to the Zn 2p, Pb 4f, and S 2p spectra. Gaussian-Lorentzian functions were used for spectral deconvolution. High-resolution spectra were obtained using a monochromatic Al Kα source, with calibration based on the Au $4f_{7/2}$ peak at 83.8 eV.

2.4. Atomic force microscopy (AFM)

Sphalerite and galena crystals were embedded in epoxy resin (Struers, Germany) and polished to achieve a mirror-like surface finish using a Tegramin-25 polishing machine (Struers, Germany). The polished surfaces were then treated with $Pb(NO_3)_2$, OA, and PAX under flotation conditions at pH 9 (as illustrated in Fig. 2A). Surface topography was analyzed using an atomic force microscope (Nano Navi S-image, Seiko Instruments Inc., Japan). Measurements were conducted using an SN-AF03 micro cantilever (Hitachi High-Tech Science Co., Ltd., Japan) in the treatment solution, with a scan speed of 0.5 Hz over a 20 × 20 μm area.

3. Results and discussion

3.1. Single mineral flotation tests

3.1.1. Effect of pH on mineral floatability

The flotation behaviors of Pb-activated sphalerite and galena under various pH conditions were investigated. Fig. 3. shows the effect of pulp pH on the floatability of single minerals in flotation tests before and after OA treatment. As can be observed in Fig. 3A, the recovery of both sphalerite and galena decreased as the pH increased from 6 to 11. For instance, at a pulp pH of 6, both Pb-activated sphalerite and galena exhibited excellent flotation recoveries of 73.2 % and 94.5 %, respectively. However, as the pH increased to 8 and 9, the recovery of sphalerite decreased to 35.0 %. Beyond pH 9, sphalerite recovery declined further to 16.7 % at pH 10 and 11.5 % at pH 11. The recovery of galena showed a gradual decline with increasing pH, decreasing from 71.5 % at pH 8 to 61.0 % at pH 9 and ultimately decreasing to 50.5 % at pH 11. The declining recovery of sphalerite and galena with increasing pH is likely due to the increased presence of hydroxyl ions (OH^-), which form hydrophilic metal hydroxide precipitates on mineral surfaces [7,10,18].

Fig. 3B demonstrates the effect of 0.56 mM OA on the flotation of Pb-activated sphalerite and galena over a pH range of 6–11. Flotation tests showed that at pH 6, sphalerite recovery was 59.0 %, while galena recovery remained largely unaffected at 93.4 %. As the pH increased to 9, the floatability of sphalerite further declined to 20 %, while galena recovery dropped to 58.7 %. These results indicate that OA can prevent Pb activation on the sphalerite surface, especially under mildly alkaline conditions, thereby reducing its flotation.

3.1.2. Effect of OA concentration on mineral floatability

To further evaluate the effect of OA, flotation tests were conducted using various OA concentrations to assess its impact on the recovery of Pb-activated sphalerite and galena. Fig. 4. displays the effect of OA concentration on the flotation recoveries of sphalerite and galena at pH 6 and pH 9. At pH 6 (Fig. 4A), the flotation recovery of Pb-activated sphalerite decreased from 73.2 % to 55.0 % after the addition of 0.14 mM OA. The recovery of Pb-activated sphalerite then fluctuated slightly with increasing OA concentrations. In contrast, the flotation recovery of galena at pH 6 ranged from 94.5 % to 83.3 % after the addition of OA, up to 0.56 mM.

At pH 9 (Fig. 4B), Pb-activated sphalerite recovery decreased with increasing OA concentrations. For example, recovery decreased from 35.6 % to 32.4 % after treatment with 0./28 mM OA and further declined to 18.3 % at 0.56 mM OA. However, adding 1.12 mM OA had an insignificant effect on sphalerite recovery. Fig. 4B also shows that galena recovery fluctuated between 60 % and 70 % with increasing OA concentrations at pH 9, with no clear detrimental effects. These results indicate that OA significantly reduced Pb-activated sphalerite recovery at 0.56 mM, while galena

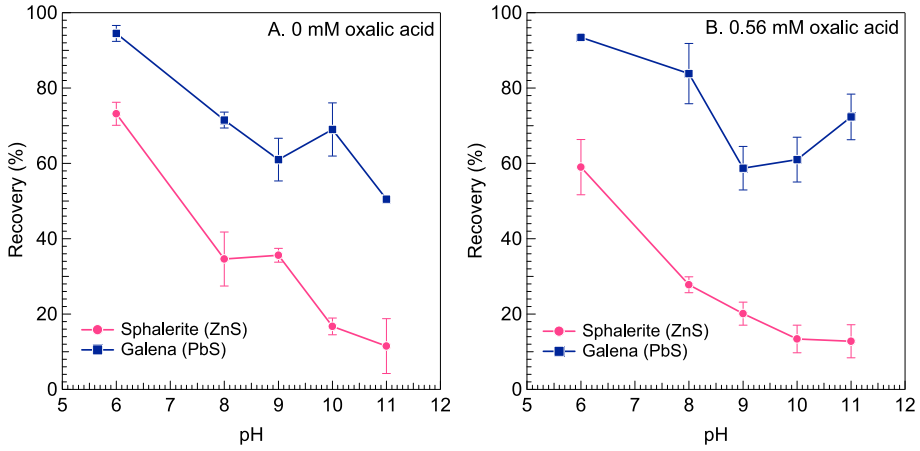

Fig. 3. Effect of pH on the flotation recovery of Pb-activated sphalerite and galena (A) before and (B) after treatment with 0.56 mM OA in 0.12 mM $Pb(NO_3)_2$ and 30 g/t PAX.

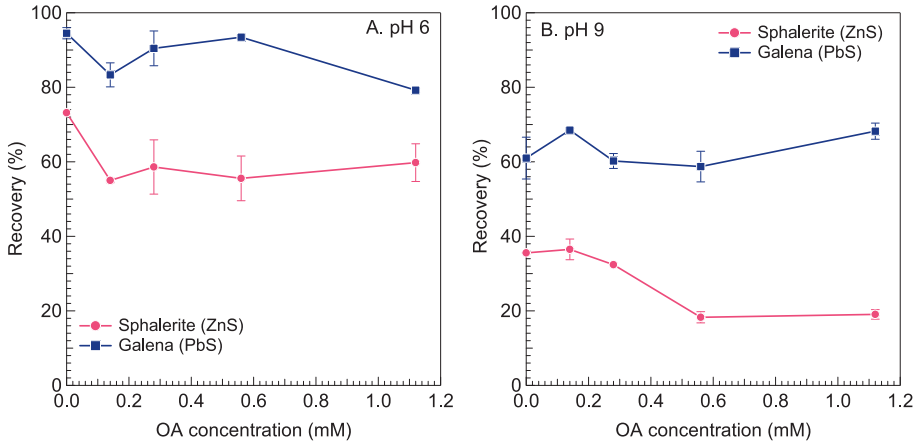

Fig. 4. Effect of OA concentration on flotation recovery of Pb-activated sphalerite and galena at (A) pH 6 and (B) pH 9 in 0.12 mM $Pb(NO_3)_2$ and 30 g/t PAX.

recovery remained relatively stable. This suggests that OA may be effective in selectively preventing the surface activation of sphalerite.

3.2. Mixed mineral flotation tests

Since collector concentration greatly affects mineral flotation recovery, it is important to investigate how different PAX concentrations impact the flotation of sphalerite and galena. To explore the potential of OA for the selective separation of Pb-activated sphalerite from galena, flotation tests were conducted using artificial mixtures at pH 9 and 0.56 mM OA with varying PAX concentrations. Fig. 5 A presents the flotation recovery data for sphalerite and galena without OA treatment. At 30 g/t PAX, the sphalerite and galena recoveries were 57.9 % and 87.9 %, respectively, yielding a Pb-Zn separation efficiency of 30.0 %. However, when the PAX concentration was increased to 120 g/t, sphalerite recovery increased significantly to 73.1 %, while galena recovery slightly decreased to 82.5 %. This suggests that higher PAX concentrations primarily enhanced the recovery of Pb-activated sphalerite while slightly reducing galena recovery, ultimately lowering the Pb-Zn separation efficiency to 9.4 %. These results confirm that the separation of Pb-activated sphalerite and galena remains a challenge.

Fig. 5B shows the flotation recovery of sphalerite and galena after treatment with 0.56 mM OA. At 30 g/t PAX, the recoveries of sphalerite and galena were 27.8 % and 76.1 %, respectively. Consequently, the Pb-Zn separation efficiency significantly improved from 30.0 % (without OA) to 48.2 % after OA treatment. This suggests that OA effectively inhibits Pb activation on sphalerite, leading to its selective depression. Increasing the PAX dosage to 120 g/t further enhanced galena recovery from 76.1 % to 83.0 %, while sphalerite recovery declined from 27.8 % to 17.0 %. As a result, the Pb-Zn separation efficiency further increased to 66.3 %. This improvement can be attributed to the high affinity of PAX for galena, which increased its recovery, while OA selectively interacted with sphalerite, reducing its affinity for PAX. This allowed for better selectivity in the mixed flotation system. In addition, the mixed flotation system demonstrated higher selectivity for OA compared to the single mineral flotation test. This is likely due to the deactivation of sphalerite and the inhibition of PAX adsorption, which will have increased the availability of PAX for interaction with galena.

3.3. FTIR spectroscopy analysis

Fig. 6. shows the FTIR spectra in the range of 600 cm^{-1} to 1800 cm^{-1} for PAX, PbOx, PbAX, and PbOx-AX as a reference for interpreting the FTIR spectra of treated minerals. The assignments of the different characteristic peaks are in reasonable agreement with those reported in the literature for similar functional groups, as presented in Table 1. For the PAX spectrum, characteristic peaks at 1070 and 1134 cm^{-1} are assigned to C=S and C-O-C stretching

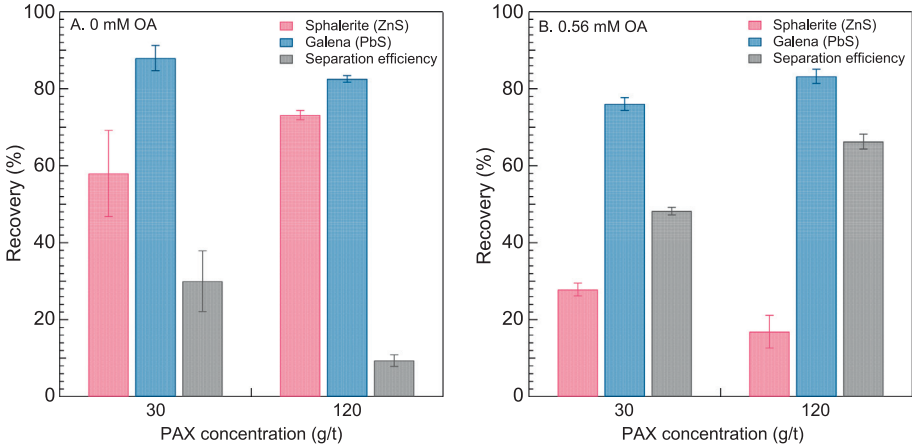

Fig. 5. Flotation recovery of sphalerite and galena in response to varying PAX concentrations (30–120 g/t PAX) (A) before and (B) after treatment with 0.56 mM OA in 0.12 mM $Pb(NO_3)_2$ at pH 9.

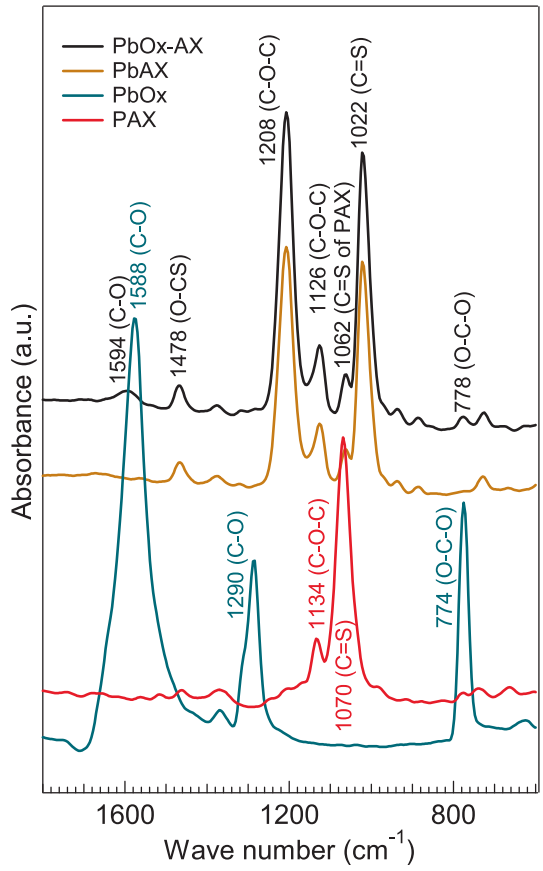

Fig. 6. FTIR spectra of potassium amyl xanthate (PAX), lead oxalate (PbOx), lead xanthate (PbAX), and the reaction product of PbOx with PAX (lead oxalate-amyl xanthate; PbOx-AX).

Table 1
Identification and interpretation of peak assignments and main functional groups in FTIR spectra from Fig. 6.

Compound	Main functional groups	Wavenumber (cm^{-1})	Ref
PAX	C=S stretching vibration	1070	[51]
	C-O-C symmetric vibration	1134	[52]
PbAX	C=S stretching vibration	1022, 1062	[55]
	C-O-C stretching vibration	1208, 1126	[54]
	O-CS bending vibration	1478	[55]
PbOx	O-C-O stretching vibration	774	[43]
	C-O antisymmetric stretching vibration	1290, 1588	[43]
PbOx-AX	C=S stretching vibration	1022, 1062	This study
	C-O-C stretching vibration	1208, 1126	This study
	O-CS bending vibration	1478	This study
	O-C-O stretching vibration	778	This study
	C-O antisymmetric stretching vibration	1594	This study

and symmetric vibrations, which are in agreement with previous findings about the structure of PAX [51,52]. In the PbAX spectrum, the interaction between PAX and Pb^{2+} ions results in shifts in the characteristic absorbance bands of PAX, indicating the formation of PbAX, as shown in Equation (2). The PbAX peaks are assigned as follows: the bands at 1022 and 1062 cm^{-1} correspond to the stretching vibrations of C=S in PbAX and the remaining PAX, while the bands at 1126 and 1208 cm^{-1} correspond to C-O-C stretching vibration. The band at 1478 cm^{-1} corresponds to the O-CS bending vibration of PbAX. These bands show no indication of dixanthogen formation [53]. These observations are consistent with previous studies and confirm the assignment of PbAX peaks [54,55].

The FTIR spectrum of chemically synthesized PbOx (Fig. 6) shows high intensity bands at 1290 and 1588 cm^{-1}, which correspond to the antisymmetric C-O stretching vibration. Meanwhile, the band at 774 cm^{-1} corresponds to the O–C–O stretching vibration. All peaks are identical to the spectra of PbOx reported in the literature [43], which confirms the complexation of Pb^{2+} and OA. In the presence of PAX and PbOx, the spectrum of the PbOx-AX complex exhibits the same distinctive peaks of xanthate (PbAX) at 1022, 1062, 1208, 1126, and 1478 cm^{-1}, with no shift in the wavenumbers. However, the peaks of PbOx at 1588 cm^{-1} and 774 cm^{-1} nearly vanish and shift to higher wavenumbers, 1594 cm^{-1} and 778 cm^{-1}, respectively. The displacement of PbOx peaks indicates a chemical interaction between PbOx and PAX, with the strong chemical bonds of Pb and amyl xanthate (AX) arising from the high affinity of AX for lead. This implies that PAX has a high affinity to react with PbOx, forming a novel compound, (Pb$(C_2O_4)(CH_3(CH_2)_4OCS_2)$) or PbOx-AX, which shows similarity to PbAX as it exhibits the same distinctive peaks of xanthate.

Fig. 7. shows the FTIR spectra in the range of 600 cm^{-1} to 1800 cm^{-1} of sphalerite and galena before and after treatment under various conditions. The spectrum of sphalerite treated with PAX (Sp + PAX) showed no obvious peaks for PAX adsorption due to the high solubility and instability of zinc xanthate on the sphalerite surface. In contrast, the spectrum of sphalerite treated with Pb$(NO_3)_2$ followed by PAX (Sp + Pb + PAX) showed peaks at 1022 and 1208 cm^{-1} with strong intensity, corresponding to the adsorption of PAX on the sphalerite surface and confirming the surface activation of sphalerite by lead, which causes the flotation of sphalerite at pH 9.

The spectrum of the Pb-activated sphalerite treated with OA and PAX (Sp + Pb + OA + PAX) showed adsorbed PAX peaks with increased intensity at 1022, 1062, 1126, and 1208 cm^{-1}. These absorbance peaks may have been caused by PAX adsorption on the surface of sphalerite or on the surface of PbOx precipitates, which were formed as the reaction products between Pb$(NO_3)_2$ and OA, as shown by Equation (3) and Fig. 6 To confirm this, the PbOA-AX precipitates were first formed and then followed by the addition of sphalerite powder into the mixture. The FTIR spectrum was then collected and labelled as Pb + OA + PAX + Sp. As can be observed in Fig. 7A, a similar spectrum was obtained with slightly lower intensity compared to that of the Sp + Pb + OA + PAX spectrum. This result indicates that the absorbance bands are predominantly caused by the adsorption of PAX on PbOx precipitates, forming a novel compound PbOx-AX rather than direct adsorption on the sphalerite surface. Furthermore, according to the reference spectra of PbOx-AX (Fig. 6), PAX has a high affinity to react with PbOx.

Fig. 7B shows the FTIR spectra of galena under various conditions before and after OA treatment. The spectrum of galena treated with PAX (Ga + PAX) showed no obvious peaks for adsorbed PAX, likely due to the low concentration of PAX on the galena surface. However, the addition of Pb$(NO_3)_2$ promoted the adsorption of PAX on the galena surface, as indicated by the peaks at 1022, 1126, and 1208 cm^{-1} in the spectrum of Ga + Pb + PAX. This result is likely caused by the reaction between Pb^{2+} ions and AX^- ions, forming PbAX on the surface of the galena.

The spectrum of Pb-activated galena treated with OA (Ga + Pb + OA + PAX) showed PAX peaks with increased intensity at 1022, 1062, 1126, and 1208 cm^{-1}. These peaks can be attributed to adsorbed PAX on the galena surface and/or due to PAX adsorption on the PbOx precipitates, as discussed previously. To clarify this spectrum, galena was added after the formation of Pb-Ox-AX precipitates, and the spectrum of Pb + OA + PAX + Ga was obtained. In contrast, the absorbance peaks in the spectrum of Pb + OA + PAX +

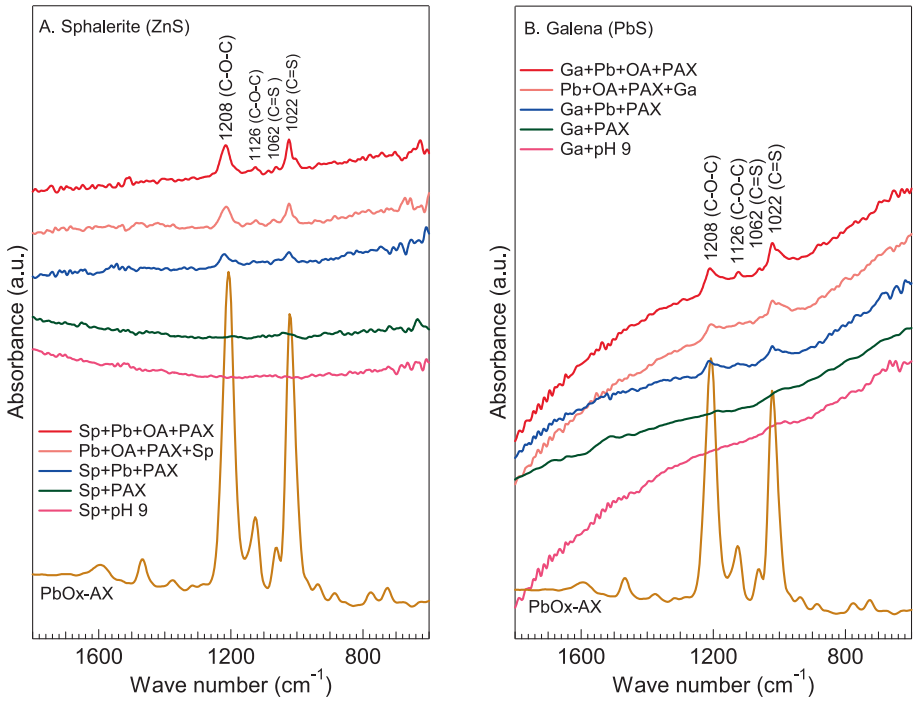

Fig. 7. FTIR spectra of (A) sphalerite and (B) galena before and after treatment under various conditions: 0.2 mM $Pb(NO_3)_2$, 5 mM OA, and 5 mM PAX. The PbOx-AX spectrum is shown as a reference.

Ga have lower intensities compared to those in the spectrum of Ga + Pb + OA + PAX. This result indicates that the absorbance bands at 1022, 1062, 1126, and 1208 cm^{-1} in the spectrum of Ga + Pb + OA + PAX were caused by a combination of PAX adsorption on Pb-Ox precipitates and direct PAX adsorption on the galena surface.

3.4. XPS analysis

XPS analysis was performed to analyze the surface chemical species for the PbAX, PbOx, and PbOx-AX precipitates as a reference for interpreting the XPS spectra of treated minerals. Fig. 8. shows the high-resolution spectra of Pb 4f for PbAX, PbOx, and PbOx-AX and S 2p for PbAX and PbOx-AX. Fig. 8A shows the Pb 4f spectrum of PbAX with doublet peaks at 137.9 eV and 142.8 eV, which are characteristic of Pb in lead xanthate. Additionally, the S 2p spectra of PbAX show binding energies of 162.0 eV and 163.2 eV for sulfur in lead xanthate [56].

The Pb 4f spectrum of PbOx contains two peaks of Pb $4f_{7/2}$ and Pb $4f_{5/2}$ at binding energy positions of 138.7 eV and 143.6 eV, respectively. The observed signals at these binding energy positions seem to correspond to Pb(II) bonding with oxalate ($(COO)_2Pb$) [57]. The interaction of PAX with PbOx precipitates shifted the Pb $4f_{7/2}$ peak of PbOx from 138.7 eV to 138.0 eV, which is relatively close to the Pb $4f_{7/2}$ peak of PbAX at 137.9 eV. This result confirms the FTIR findings, which indicate that the interaction of PAX with PbOx precipitates predominantly forms a xanthate complex rather than an oxalate complex. This interaction likely involves the adsorption of PAX onto the surface of PbOx. Furthermore, the S 2p spectra of PbAX and PbOx-AX (Fig. 8B) showed similar binding energies for the S $2p_{3/2}$ and S $2p_{1/2}$ peaks at 162.0 eV and 163.2 eV, respectively. This provides further evidence of the similarity in the chemical composition of both PbAX and PbOx-AX, which is consistent with the FTIR data.

To further investigate the formation of surface chemical species on activated sphalerite and galena before and after OA treatment, high-resolution XPS spectra, binding energies, and the relative contents of surface minerals were analyzed. Fig. 9. shows the Zn 2p and S 2p high-resolution spectra of sphalerite. Fig. 9 A shows the Zn 2p spectrum of untreated sphalerite, in which the prominent peak near 1021.6 eV is assigned to Zn(II) in ZnS, which is consistent with previously reported values [19,58,59]. After PAX treatment, a shoulder peak appeared at 1019.2 eV, which is assigned to the Zn(I) species, as reported by Le et al. [60]. In addition, the main peak slightly shifted to a lower binding energy from 1021.6 eV to 1021.4 eV. This shoulder peak indicates that the xanthate reaction with the sphalerite surface produced a zinc-deficient surface. A similar shoulder peak was observed when the Pb-activated sphalerite was treated with PAX with and without OA. However, the intensity of the main peak of Zn 2p decreased after Pb activation with and without OA, probably resulting from the precipitation of Pb species on the surface of sphalerite, as confirmed by Pb 4f spectra shown in Fig. 10.

The high-resolution S 2p spectra of sphalerite after different treatments are shown in Fig. 9B. The main peak of untreated sphalerite at 161.5 eV is assigned to S^{2-} of sphalerite [58,61]. After PAX treatment, there was a slight shift in the S^{2-} binding energy to 161.6 eV, without any new peak formation, indicating the absence of xanthate adsorption. On the other hand, a new peak at 162.0 eV appeared after the addition of PAX to Pb-activated sphalerite. This peak corresponds with sulfur from lead xanthate (PbAX) precipitation, as shown in Fig. 8B. After OA treatment on Pb-activated sphalerite, followed by PAX, the S 2p spectra showed a newly formed peak at 162.0 eV, which is attributed to the formation of the PbOx-AX complex on sphalerite.

The high-resolution Pb 4f spectra of sphalerite under different treatments are presented in Fig. 10. The deconvoluted spectrum of untreated sphalerite and sphalerite treated with PAX shows the absence of Pb species. Fig. 10 also shows the Zn 3 s peak at 139.6 eV, which agrees with the previously reported work by Aikawa et al. [62]. Pb-activated sphalerite treated with PAX shows newly formed Pb $4f_{7/2}$ peaks at 138.0 eV and 138.4 eV, which cor-

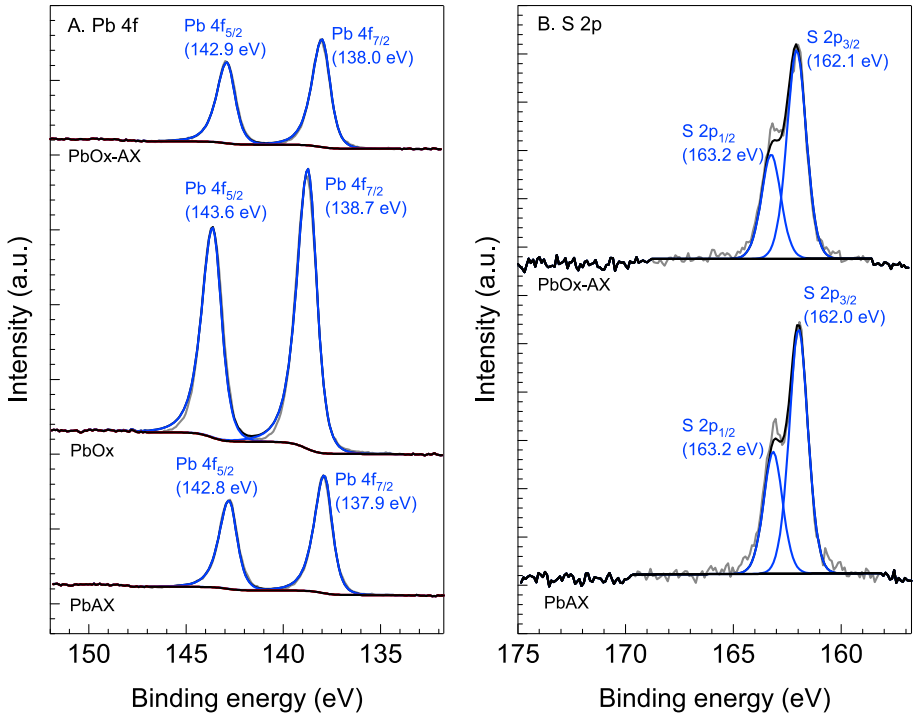

Fig. 8. High-resolution XPS spectra of (A) Pb 4f and (B) S 2p of lead amyl xanthate (PbAX), lead oxalate (PbOx), and lead oxalate-amyl xanthate (PbOx-AX).

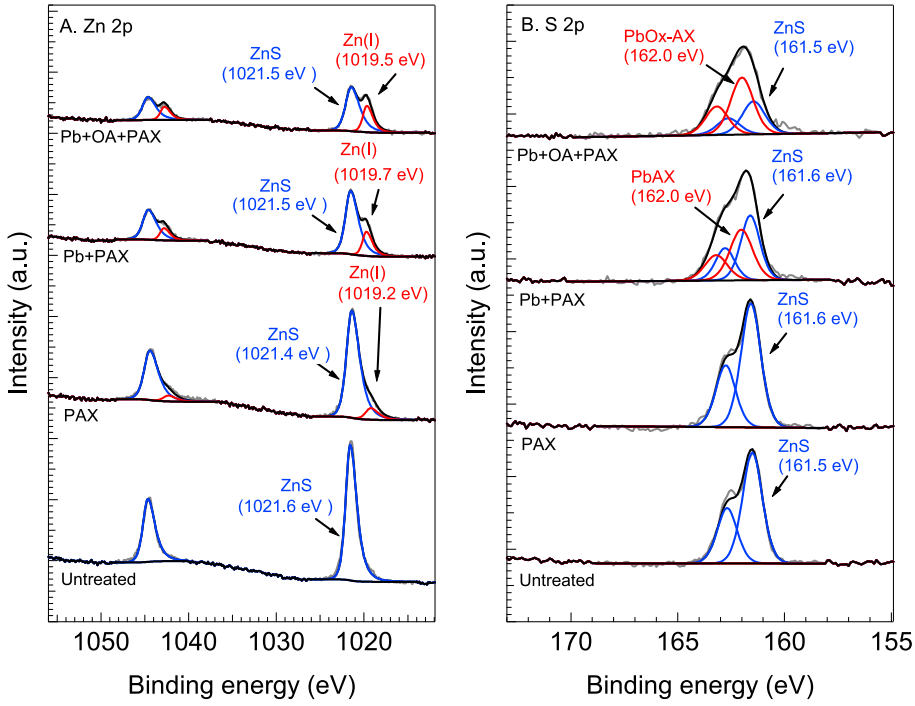

Fig. 9. High-resolution (A) Zn 2p and (B) S 2p spectra of sphalerite under various treatments in 0.2 mM $Pb(NO_3)_2$, 5 mM PAX, and 5 mM OA at pH 9.

respond to lead xanthate (Pb-AX) precipitation [56] and residual Pb $(NO_3)_2$ on the sphalerite surface, respectively [63]. However, after OA treatment, the newly formed peak at 138.0 eV is assigned to the PbOx-AX complex, based on the reference in Fig. 8A and FTIR results.

Fig. 11A shows the Pb 4f spectra of galena under different treatments. The spectrum of untreated galena consists of two characteristic peaks at 137.4 eV and 138.1 eV, corresponding to metallic PbS and lead oxides, respectively, as reported in previous studies [58]. After PAX treatment, there was no significant change in Pb binding energy compared to untreated galena. This may be due to the low concentration of lead, which is consistent with the FTIR results. On the other hand, XPS analysis revealed that the addition of PAX after lead activation formed lead xanthate (PbAX), as indicated by the

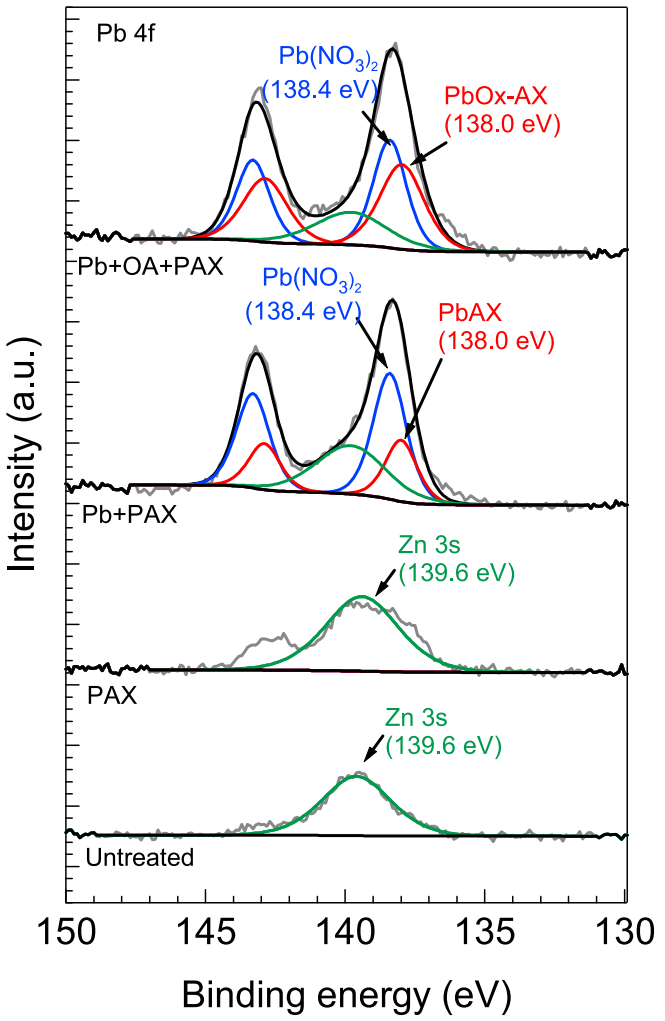

Fig. 10. High-resolution Pb 4f spectra of sphalerite under different treatments in 0.2 mM $Pb(NO_3)_2$, 5 mM PAX, and 5 mM OA at pH 9.

peak at 138.0 eV, which matches the binding energy of PbAX in the reference shown in Fig. 8A. A similar spectrum was obtained after OA treatment on Pb-activated galena, followed by PAX treatment. However, the peak at 138.0 eV exhibited a higher intensity in the presence of OA. This is likely due to the formation of PbOx-AX.

Fig. 11B shows the S 2p spectra of galena under various treatments. The spectrum of pure galena displays a prominent main peak at 160.6 eV, which is attributed to S^{2-}in PbS [58]. After PAX treatment, no new peaks were formed, but the binding energy of the S 2p peak shifted slightly from 160.6 eV to 160.7 eV. In contrast, the XPS spectrum of Pb-activated galena treated with PAX showed a new peak at a binding energy of 162.2 eV, which is in agreement with the binding energy of lead xanthate reported by Laajalehto et al.[56], as well as with the S 2p peak of PbAX in the reference spectra shown in Fig. 8B. There was no change in the binding energy of S^{2-} in the galena after treatment with PAX. However, the S 2p spectra broadened after Pb activation, with and without OA, followed by PAX treatment. After OA treatment, the deconvolution results indicated that a new peak at 162.1 eV could be fitted to the spectra. This new peak is assigned to sulfur from the xanthate group in PbAX and PbOx-AX, supporting the Pb 4f spectra and FTIR results.

3.5. AFM

Fig. 12 presents AFM images of galena and sphalerite subjected to various treatments under flotation test conditions. Fig. 12A(i) and 12B(i) show the clean, untreated surfaces of galena and sphalerite, respectively. After the treatment using 120 g/t PAX, both mineral surfaces remained clean, as seen in Fig. 12A(ii) and 12B (ii). However, when treated with $Pb(NO_3)_2$ followed by PAX, the surfaces of galena and sphalerite displayed distinct white spots, as illustrated in Fig. 12A(iii) and 12B(iii). These white spots are likely PbAX, as confirmed by the FTIR and XPS results.

Fig. 12A(iv) indicates that the white spots on the galena surface persisted even after OA treatment, suggesting that PbAX strongly adheres to the galena surface. In contrast, Fig. 12B(iv) shows that OA treatment effectively removed most white spots from the sphalerite surface. This suggests that OA reacted with Pb ions, forming precipitates that detached from the sphalerite surface. This process prevents Pb activation, effectively cleaning the surface and hindering PAX adsorption. The AFM observations are consistent with the conclusions drawn from the FTIR and XPS analyses.

3.6. Proposed mechanism and separation process

Based on flotation tests and surface spectroscopy analyses, a model for the selective separation of sphalerite using OA in Pb-Zn flotation is proposed (Fig. 13). Initially, Pb ions (Pb^{2+}) dissolve from the galena surface and migrate to the sphalerite surface (Step 1). The Pb^{2+} ions activate the sphalerite surface, primarily by forming lead sulfide (PbS) precipitates (Step 2), which react with amyl xanthate ions (AX^-) to form PbAX (Step 3). This process facilitates sphalerite flotation, as shown in Equation (4).

The activation occurs through ion exchange, in which Pb^{2+} ions replace Zn^{2+} ions on the sphalerite surface, as described in Equation (5) [14].

$$ZnS_{(S)} + Pb^{2+} \rightarrow PbS_{(s)} + Zn^{2+} \quad (5)$$

Alternatively, Pb^{2+} activation may involve the formation of lead oxide ($Pb(OH)_2$) species on the sphalerite surface $ZnS/Zn(OH)_2$, as shown in Equation (6) [3].

$$ZnS/Zn(OH)_2 + Pb(OH)_2 \rightarrow ZnS/Zn - O - Pb^{+} + H_2O \quad (6)$$

These oxide species serve as attachment points for xanthate binding; as a result, they increase sphalerite floatability because the PbS-like compound has a higher affinity with AX^- ions than sphalerite [14].

While $Pb2^+$ significantly activates sphalerite, it has minimal impact on galena [13]. Galena's natural hydrophobicity and favorable response to xanthate collectors allow AX^- ions to adsorb directly onto its surface (Step 4) or via Pb(II) species formed on it (Step 3) [56].

Fig. 13B illustrates the effect of OA treatment on Pb-activated sphalerite and galena. At pH values above 4.19, OA exists as oxalate ions ($C_2O_4^{2-}$, Ox^{2-}) [29]. OA reacts with Pb^{2+} ions, forming PbOx precipitates that detach from the sphalerite surface (Step 5). This effectively cleans the sphalerite surface by removing Pb^{2+} ions, hindering PAX adsorption, and exposing the hydrophilic surface, leading to depression of the surface. AX^- ions further react with PbOx precipitates to form dispersed PbOx-AX complexes (Step 6), which inhibit sphalerite flotation. On the galena surface, a similar PbOx-AX complex forms. However, galena's structural properties allow AX^- ions to adsorb readily, ensuring it remains floatable after OA treatment.

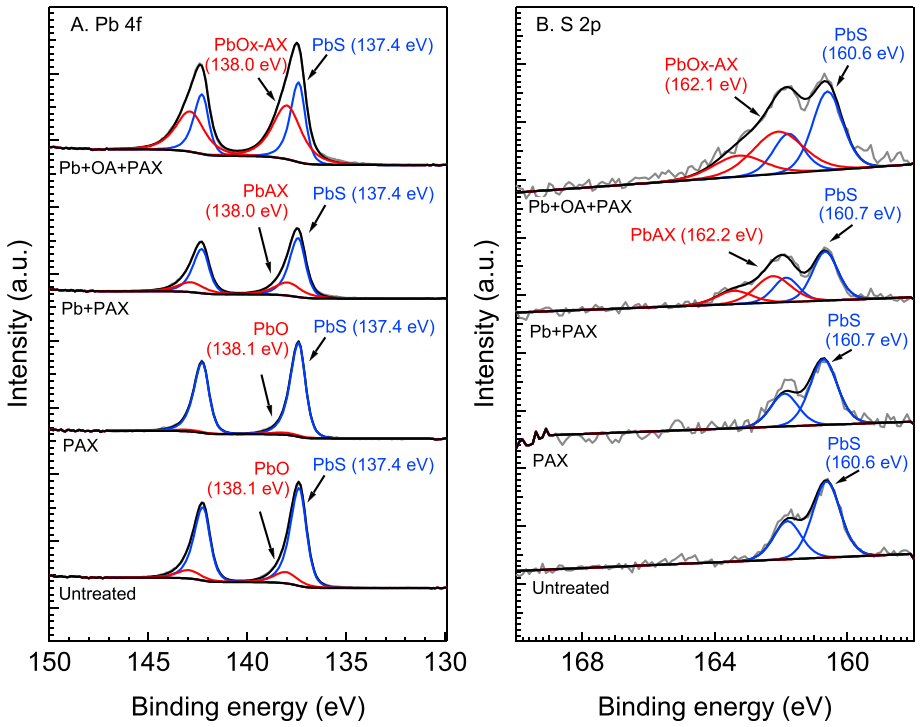

Fig. 11. High-resolution (A) Pb 4f and (B) S 2p spectra of galena under various treatments in 0.2 mM $Pb(NO_3)_2$, 5 mM PAX, and 5 mM OA at pH 9.

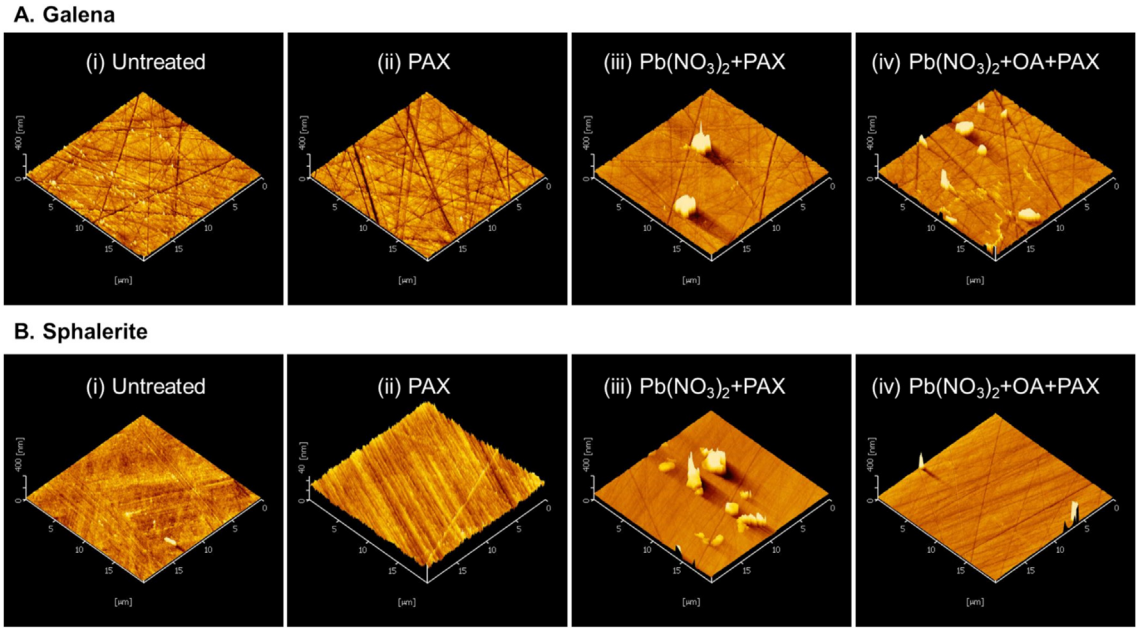

Fig. 12. Surface topography of galena (A) and sphalerite (B) after treatment under different conditions: (i) untreated (pH 9), (ii) 120 g/t PAX, (iii) 0.12 mM $Pb(NO_3)_2$ + 120 g/t PAX, and (iv) 0.12 mM $Pb(NO_3)_2$ + 0.56 mM OA + 120 g/t PAX.

4. Conclusion

In this study, OA was used for the first time as an environmentally friendly reagent to selectively deactivate the sphalerite surface in Pb-Zn flotation separation. Single and mixed flotation tests demonstrated that effective separation of sphalerite and galena could be achieved under mildly alkaline conditions. Specifically, OA at 0.56 mM reduced sphalerite recovery to 20 %, while galena recovery was 58.7 % in single-mineral flotation tests. In artificial mixtures, OA treatment resulted in recoveries of 83 % for galena and 17 % for sphalerite. FTIR and XPS analyses showed that OA reacts with Pb^{2+} ions on the sphalerite surface, forming a

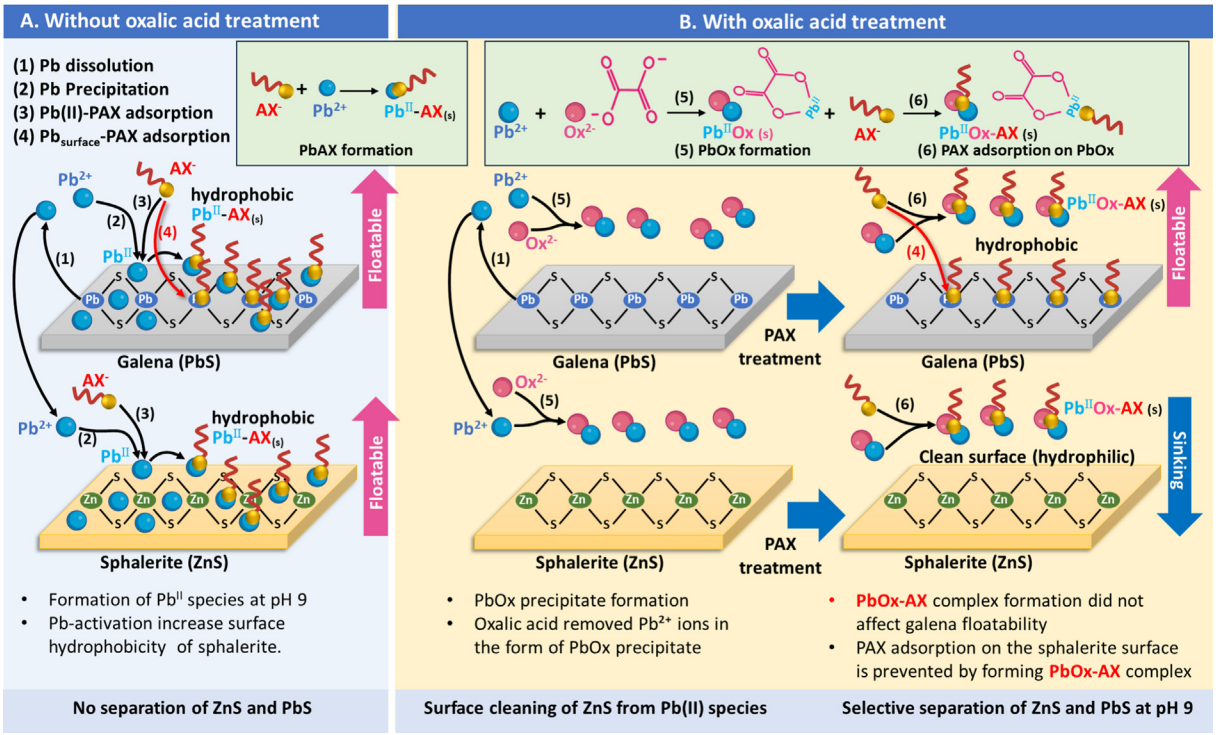

Fig. 13. Proposed mechanism for the selective separation of sphalerite and galena: (A) without OA treatment and (B) after OA treatment.

Pb^{II}-Ox precipitate that detaches from the surface, effectively cleaning it and preventing the adsorption of PAX. This leads to the depression of sphalerite floatability, while the formation of PbOx-AX does not significantly affect galena floatability. In summary, these findings identify a novel reagent for the selective deactivation of sphalerite while maintaining the floatability of galena, paving the way for more environmentally sustainable flotation processes in Pb-Zn separation. Further studies are needed to investigate the structure of this novel PbOx-AX complex.

CRediT authorship contribution statement

Doaa Ashraf Eladl: Writing – original draft, Visualization, Methodology, Investigation, Formal analysis, Data curation. **Gde Pandhe Wisnu Suyantara:** Writing – review & editing, Writing – original draft, Validation, Supervision, Methodology, Funding acquisition, Conceptualization. **Hajime Miki:** Writing – review & editing, Validation, Supervision, Project administration, Funding acquisition. **Akbarshokh Ulmaszoda:** Validation, Methodology, Data curation. **Naoko Okibe:** Writing – review & editing, Validation, Supervision, Project administration, Methodology, Funding acquisition, Conceptualization.

Declaration of competing interest

The authors declare that they have no known competing financial interests or personal relationships that could have appeared to influence the work reported in this paper.

Acknowledgements

This work was supported by a Grant-in-Aid for Science Research (JSPS KAKENHI) from the Japan Society for the Promotion of Science (JSPS) – Japan [Grant numbers JP23H03815, JP22H00310, and 20H00647]. The first author would like to thank the Rotary Yoneyama Memorial Foundation for providing the scholarship. The X-ray photoelectron spectroscopy study was funded by the Japanese Ministry of Education, Culture, Sports, Science, and Technology (MEXT) under the "Advanced Research Infrastructure for Materials and Nanotechnology in (ARIM)" [Grant number JPMXP1222KU1020].

References

[1] K.H. Rao, Challenges in Sulphide Mineral Processing, Open Miner. Process. J. 4 (2011) 7–13. https://doi.org/10.2174/1874841400110401007.
[2] X. Sun, R.-Y. Li, H.-Y. Sun, P.H. Olin, M. Santosh, B. Fu, J. Deng, Genesis of Pb–Zn-Ag-Sb mineralization in the Tethys Himalaya, China: Early magmatic-hydrothermal Pb–Zn(-Ag) mineralization overprinted by Sb-rich fluids, Miner. Deposita 59 (2024) 1275–1293. https://doi.org/10.1007/s00126-024-01264-5.
[3] J. Liu, M. Ejtemaei, A.V. Nguyen, S. Wen, Y. Zeng, Surface chemistry of Pb-activated sphalerite, Miner. Eng. 145 (2020) 106058. https://doi.org/10.1016/j.mineng.2019.106058.
[4] B. Huang, H. Lai, J. Deng, H. Xu, G. Fan, Study on the Interaction between Galena and Sphalerite During Grinding Based on the Migration of Surface Components, ACS Omega 4 (2019) 12489–12497. https://doi.org/10.1021/acsomega.9b01173.
[5] M. Liu, C. Cheng, Z. Qiu, L. Yang, S. Liu, G. Liu, Weak alkaline flotation separation of galena from sphalerite with 6-butylamino-1,3,5-triazine-2(1H)-thione-4-thiol sodium, Appl. Surf. Sci. 663 (2024) 160162. https://doi.org/10.1016/j.apsusc.2024.160162.
[6] L. Wang, Y. Zhang, R. Han, X. Li, LA-ICP-MS analyses of trace elements in zoned sphalerite: A study from the Maoping carbonate-hosted Pb-Zn(-Ge) deposit, southwest China, Ore Geol. Rev. 157 (2023) 105468. https://doi.org/10.1016/j.oregeorev.2023.105468.
[7] Y. Hu, M. Wu, R. Liu, W. Sun, A review on the electrochemistry of galena flotation, Miner. Eng. 150 (2020) 106272. https://doi.org/10.1016/j.mineng.2020.106272.
[8] Z. Zhang, Q. Sun, S. Liu, Z. Lu, X. Niu, M.M.M. Ahmed, G. Liu, The selective flotation separation of galena from sphalerite with a novel collector of 5-amyl-1, 2, 4-triazole-3-thione, J. Mol. Liq. 332 (2021) 115902. https://doi.org/10.1016/j.molliq.2021.115902.
[9] X. Niu, J. Chen, Y. Li, L. Xia, L. Li, H. Sun, R. Ruan, Correlation of surface oxidation with xanthate adsorption and pyrite flotation, Appl. Surf. Sci. 495 (2019) 143411. https://doi.org/10.1016/j.apsusc.2019.07.153.
[10] L. Kong, X. Fu, L. Lu, R. Wang, H. Wang, Y. Meng, X. Zhang, A novel selective galena collector based on modified dithiophosphate in Pb-Zn flotation

separation and its adsorption mechanism, Adv. Powder Technol. 35 (2024) 104489. https://doi.org/10.1016/j.apt.2024.104489.
[11] A. Sarvaramini, F. Larachi, B. Hart, Collector attachment to lead-activated sphalerite – Experiments and DFT study on pH and solvent effects, Appl. Surf. Sci. 367 (2016) 459–472. https://doi.org/10.1016/j.apsusc.2016.01.213.
[12] Y. Feng, Y. Chen, J. Chen, The mechanism of surface activation in sphalerite by metal ions with d10 electronic configurations: Experimental and DFT study, Appl. Surf. Sci. 649 (2024) 159181. https://doi.org/10.1016/j.apsusc.2023.159181.
[13] Y. Liu, Z. Wei, C. Xue, Selective depression of Pb^{2+}-activated sphalerite by potassium ferricyanide in Pb-Zn sulfides flotation separation, Miner. Eng. 182 (2022) 107558. https://doi.org/10.1016/j.mineng.2022.107558.
[14] K. Aikawa, M. Ito, A. Kusano, I. Park, T. Oki, T. Takahashi, H. Furuya, N. Hiroyoshi, Flotation of Seafloor Massive Sulfide Ores: Combination of Surface Cleaning and Deactivation of Lead-Activated Sphalerite to Improve the Separation Efficiency of Chalcopyrite and Sphalerite, Metals 11 (2021) 253. https://doi.org/10.3390/met11020253.
[15] X.-H. Wang, K.S.E. Forssberg, The solution electrochemistry of sulfide-xanthate-cyanide systems in sulfide mineral flotation, Miner. Eng. 9 (1996) 527–546. https://doi.org/10.1016/0892-6875(96)00041-6.
[16] H.E. El-Shall, D.A. Elgillani, N.A. Abdel-Khalek, Role of zinc sulfate in depression of lead-activated sphalerite, Int. J. Miner. Process. 58 (2000) 67–75. https://doi.org/10.1016/S0301-7516(99)00055-1.
[17] C. Wang, R. Liu, W. Sun, N. Jing, F. Xie, Q.Z.D. He, Selective depressive effect of pectin on sphalerite flotation and its mechanisms of adsorption onto galena and sphalerite surfaces, Miner. Eng. 170 (2021) 106989. https://doi.org/10.1016/j.mineng.2021.106989.
[18] Y. Chen, B. Feng, J. Peng, Z. Wang, Selective flotation of galena from sphalerite using a combination of KMnO4 and carboxylated chitosan, Appl. Surf. Sci. 602 (2022) 154412. https://doi.org/10.1016/j.apsusc.2022.154412.
[19] X. Xu, X. Zhang, Y. Zhang, X. Liu, H. He, J. Fang, P. Shen, R. Peng, J. Yu, X. Chen, D. Liu, A study on the mechanism of flotation separation between chalcopyrite and sphalerite using a novel environmental depressant derived from grape peel extract GPE, Colloids Surf. Physicochem. Eng. Asp. 681 (2024) 132772. https://doi.org/10.1016/j.colsurfa.2023.132772.
[20] X. Tan, Y. Zhu, C. Sun, X. Zhang, J. Su, Adding cationic guar gum after collector: A novel investigation in flotation separation of galena from sphalerite, Miner. Eng. 157 (2020) 106542. https://doi.org/10.1016/j.mineng.2020.106542.
[21] Y. Cui, F. Jiao, W. Qin, C. Wang, X. Li, Flotation separation of sphalerite from galena using eco-friendly and efficient depressant pullulan, Sep. Purif. Technol. 295 (2022) 121013. https://doi.org/10.1016/j.seppur.2022.121013.
[22] P. Huang, M. Cao, Q. Liu, Selective depression of sphalerite by chitosan in differential PbZn flotation, Int. J. Miner. Process. 122 (2013) 29–35. https://doi.org/10.1016/j.minpro.2013.04.010.
[23] R.K. Rath, S. Subramanian, Adsorption, electrokinetic and differential flotation studies on sphalerite and galena using dextrin, Int. J. Miner. Process. 57 (1999) 265–283. https://doi.org/10.1016/S0301-7516(99)00028-9.
[24] F. Rashchi, J.A. Finch, C. Sui, Action of DETA, dextrin and carbonate on lead-contaminated sphalerite, Colloids Surf. Physicochem. Eng. Asp. 245 (2004) 21–27. https://doi.org/10.1016/j.colsurfa.2004.05.018.
[25] F. Rashchi, J.A. Finch, Deactivation of Pb-contaminated sphalerite by polyphosphate, Colloids Surf. Physicochem. Eng. Asp. 276 (2006) 87–94. https://doi.org/10.1016/j.colsurfa.2005.10.027.
[26] N. Chen, S. Tao, K. Xiao, S. Liang, J. Yang, L. Zhang, A one-step acidification strategy for sewage sludge dewatering with oxalic acid, Chemosphere 238 (2020) 124598. https://doi.org/10.1016/j.chemosphere.2019.124598.
[27] H. Safari, M. Rezaee, S.C. Chelgani, Ecofriendly leaching agents for copper extraction—An overview of amino and organic acid applications, Green Smart, Min. Eng. 1 (2024) 336–345. https://doi.org/10.1016/j.gsme.2024.08.004.
[28] A.N. Amenaghawon, J.E. Ayere, U.O. Amune, I.C. Otuya, E.C. Abuga, C.L. Anyalewechi, O.V. Okoro, J.A. Okolie, P.K. Oyefolu, S.O. Eshiemogie, B.E. Osahon, M. Omede, S.A. Eshiemogie, S. Igemhokhai, M.O. Okedi, H.S. Kusuma, O.E. Muojama, A. Shavandi, H. Darmokoesoemo, A comprehensive review of recent advances in the applications and biosynthesis of oxalic acid from bio-derived substrates, Environ. Res. 251 (2024) 118703. https://doi.org/10.1016/j.envres.2024.118703.
[29] X. Liu, G. Huang, C. Li, R. Cheng, Depressive effect of oxalic acid on titanaugite during ilmenite flotation, Miner. Eng. 79 (2015) 62–67. https://doi.org/10.1016/j.mineng.2015.05.013.
[30] A. Verma, R. Kore, D.R. Corbin, M.B. Shiflett, Metal Recovery Using Oxalate Chemistry: A Technical Review, Ind. Eng. Chem. Res. 58 (2019) 15381–15393. https://doi.org/10.1021/acs.iecr.9b02598.
[31] W. Astuti, F. Nurjaman, F. Rofiek Mufakhir, S. Sumardi, D. Avista, K. Cleary Wanta, H., Tri Bayu Murti Petrus, A novel method: Nickel and cobalt extraction from citric acid leaching solution of nickel laterite ores using oxalate precipitation, Miner. Eng. 191 (2023) 107982. https://doi.org/10.1016/j.mineng.2022.107982.
[32] S. Kursunoglu, M. Kaya, Dissolution behavior of Caldag lateritic nickel ore subjected to a sequential organic acid leaching method, Int. J. Miner. Metall. Mater. 22 (2015) 1131–1140. https://doi.org/10.1007/s12613-015-1177-9.
[33] X. Zeng, J. Li, B. Shen, Novel approach to recover cobalt and lithium from spent lithium-ion battery using oxalic acid, J. Hazard. Mater. 295 (2015) 112–118. https://doi.org/10.1016/j.jhazmat.2015.02.064.
[34] D. Schmitz, H. Prasetyo, A. Birich, R. Yeetsorn, B. Friedrich, Co-Precipitation of Metal Oxalates from Organic Leach Solution Derived from Spent Lithium-Ion Batteries (LIBs), Metals 14 (2024) 80. https://doi.org/10.3390/met14010080.
[35] A. Szymczycha-Madeja, Kinetics of Mo, Ni, V and Al leaching from a spent hydrodesulphurization catalyst in a solution containing oxalic acid and hydrogen peroxide, J. Hazard. Mater. 186 (2011) 2157–2161. https://doi.org/10.1016/j.jhazmat.2010.11.120.
[36] O. Falyouna, M. Faizul Idham, I. Maamoun, K. Bensaida, U. Ashik, Y. Sugihara, O. Eljamal, Promotion of ciprofloxacin adsorption from contaminated solutions by oxalate modified nanoscale zerovalent iron particles, J. Mol. Liq. 359 (2022) 119323. https://doi.org/10.1016/j.molliq.2022.119323.
[37] O. Falyouna, I. Maamoun, S. Ghosh, A. Malloum, A. Othmani, O. Eljamal, T.W.M. Amen, A. Oroke, C. Bornman, S. Ahmadi, M. Hadi Dehghani, A. Hossein Mahvi, S. Nasseri, I. Tyagi, J.R. Suhas, Koduru, Sustainable technologies for the removal of Chloramphenicol from pharmaceutical industries Effluent: A critical review, J. Mol. Liq. 368 (2022) 120726. https://doi.org/10.1016/j.molliq.2022.120726.
[38] H. Zhao, F. Yang, Z. Wang, Y. Li, J. Guo, S. Li, J. Shu, M. Chen, Chlorine and heavy metals removal from municipal solid waste incineration fly ash by electric field enhanced oxalic acid washing, J. Environ. Manage. 340 (2023) 117939. https://doi.org/10.1016/j.jenvman.2023.117939.
[39] F. Vakilchap, S.M. Mousavi, S.A. Shojaosadati, Role of Aspergillus niger in recovery enhancement of valuable metals from produced red mud in Bayer process, Bioresour. Technol. 218 (2016) 991–998. https://doi.org/10.1016/j.biortech.2016.07.059.
[40] H. Huang, Y. Hu, W. Sun, Activation flotation and mechanism of lime-depressed pyrite with oxalic acid, Int. J. Min. Sci. Technol. 22 (2012) 63–67. https://doi.org/10.1016/j.ijmst.2011.07.007.
[41] R. Liao, S. Wen, Q. Feng, J. Deng, H. Lai, Activation mechanism of ammonium oxalate with pyrite in the lime system and its response to flotation separation of pyrite from arsenopyrite, Int. J. Miner. Metall. Mater. 30 (2023) 271–282. https://doi.org/10.1007/s12613-022-2505-5.
[42] G.P.W. Suyantara, A. Ulmaszoda, H. Miki, D.A. Eladl, K. Sasaki, N. Okibe, Selective depression of copper-activated pyrite by oxalic acid: Implications for enhanced chalcopyrite–pyrite separation, Powder Technol. (2025) 120681. https://doi.org/10.1016/j.powtec.2025.120681.
[43] N. Mancilla, M.C. D'Antonio, A.C. González-Baró, E.J. Baran, Vibrational spectra of lead(II) oxalate, J. Raman Spectrosc. 40 (2009) 2050–2052. https://doi.org/10.1002/jrs.2370.
[44] G.P.W. Suyantara, I.N. Rizki, A. Ulmaszoda, H. Miki, K. Sasaki, Effect of goethite (α-FeOOH) nanoparticles on the surface properties and flotation behavior of chalcopyrite, J. Environ. Chem. Eng. 11 (2023) 110006. https://doi.org/10.1016/j.jece.2023.110006.
[45] D. Berdakh, H. Miki, T. Hirajima, K. Sasaki, A. Ulmaszoda, R. Nakao, D. Ochi, Y. Aoki, G.P.W. Suyantara, Effect of oxidation treatment on the selective separation of molybdenite from chalcocite using flotation, Powder Technol. 431 (2024) 119078. https://doi.org/10.1016/j.powtec.2023.119078.
[46] G.P.W. Suyantara, T. Hirajima, H. Miki, K. Sasaki, Floatability of molybdenite and chalcopyrite in artificial seawater, Miner. Eng. 115 (2018) 117–130. https://doi.org/10.1016/j.mineng.2017.10.004.
[47] G.P.W. Suyantara, D. Berdakh, H. Miki, T. Hirajima, K. Sasaki, D. Ochi, Y. Aoki, Effect of hydrogen peroxide on selective flotation of chalcocite and enargite, Int. J. Min. Sci. Technol. 33 (2023) 703–716. https://doi.org/10.1016/j.ijmst.2023.01.002.
[48] Y. Semoto, G.P.W. Suyantara, H. Miki, K. Sasaki, T. Hirajima, Y. Tanaka, Y. Aoki, K. Ura, Effect of Sodium Metabisulfite on Selective Flotation of Chalcopyrite and Molybdenite, Minerals 11 (2021) 1377. https://doi.org/10.3390/min11121377.
[49] F. Grases, J. Ruiz, A. Costa-Bauzá, Studies on Lead Oxalate Crystalline Growth, J. Colloid Interface Sci. 155 (1993) 265–270. https://doi.org/10.1006/jcis.1993.1035.
[50] A. Robledo-Cabrera, O.A. Orozco-Navarro, A. López-Valdivieso, Solubility product and heat of formation of lead alkyl xanthates by microcalorimetric titration, Int. J. Miner. Process. 144 (2015) 65–69. https://doi.org/10.1016/j.minpro.2015.10.003.
[51] Z. Feng, Y. Zhao, J. Wang, P. Chen, J. Cao, Thiourea compounds with diverse hydrophobic group used as selective flotation collectors for galena, Miner. Eng. 207 (2024) 108575. https://doi.org/10.1016/j.mineng.2024.108575.
[52] J. Yu, X. Wu, Z. Zhao, Y. Zhu, S. Luo, Effect of a Small Amount of Iron Impurity in Sphalerite on Xanthate Adsorption and Flotation Behavior, Minerals 9 (2019) 687. https://doi.org/10.3390/min9110687.
[53] J.M. Cases, P. De Donato, FTIR analysis of sulphide mineral surfaces before and after collection: galena, Int. J. Miner. Process. 33 (1991) 49–65. https://doi.org/10.1016/0301-7516(91)90042-H.
[54] J.O. Leppinen, C.I. Basilio, R.H. Yoon, In-situ FTIR study of ethyl xanthate adsorption on sulfide minerals under conditions of controlled potential, Int. J. Miner. Process. 26 (1989) 259–274. https://doi.org/10.1016/0301-7516(89)90032-X.
[55] N. Mhonde, L. Pitkänen, K. Corin, N. Schreithofer, The Solution Interaction of Tetrathionate Ions and Sodium Isobutyl Xanthate and Its Effect on the Flotation of Galena and Chalcopyrite, Minerals 11 (2021) 204. https://doi.org/10.3390/min11020204.
[56] K. Laajalehto, P. Nowak, E. Suoninen, On the XPS and IR identification of the products of xanthate sorption at the surface of galena, Int. J. Miner. Process. 37 (1993) 123–147. https://doi.org/10.1016/0301-7516(93)90009-Y.
[57] W. Wei, X. Han, Y. Shao, W. Xie, Y. Zhang, Y. Yao, W. Zhao, R. Han, S. Li, Y. Zhang, C. Zheng, Comparing the effects of humic acid and oxalic acid on Pb(II) immobilization by a green synthesized nanocrystalline hydroxyapatite,

Chemosphere 285 (2021) 131411. https://doi.org/10.1016/j.chemosphere.2021.131411.
[58] H. Zhu, B. Yang, R. Martin, H. Zhang, D. He, H. Luo, Flotation separation of galena from sphalerite using hyaluronic acid (HA) as an environmental-friendly sphalerite depressant, Miner. Eng. 187 (2022) 107771. https://doi.org/10.1016/j.mineng.2022.107771.
[59] M.N. Islam, T.B. Ghosh, K.L. Chopra, H.N. Acharya, XPS and X-ray diffraction studies of aluminum-doped zinc oxide transparent conducting films, Thin Solid Films 280 (1996) 20–25. https://doi.org/10.1016/0040-6090(95)08239-5.
[60] T.K. Le, T.L. Nguyen, C.N. Hoang, D.K.A. Nguyen, T. Lund, H.K.H. Nguyen, T.K.X. Huynh, Formation of surface defects by thermal shock method for the improved photocatalytic activity of ZnO nanoparticles, J. Asian Ceram. Soc. 8 (2020) 193–202. https://doi.org/10.1080/21870764.2020.1720900.
[61] T. Qiu, G. Li, X. Li, H. Yan, C. Liu, Influence of high concentration Zn2+ on floatability of sphalerite in acidic system, Trans. Nonferrous Met. Soc. China 31 (2021) 2128–2138. https://doi.org/10.1016/S1003-6326(21)65643-1.
[62] K. Aikawa, M. Ito, A. Kusano, S. Jeon, I. Park, N. Hiroyoshi, Development of a Sustainable Process for Complex Sulfide Ores Containing Anglesite: Effect of Anglesite on Sphalerite Floatability, Enhanced Depression of Sphalerite by Extracting Anglesite, and Recovery of Extracted Pb2+ as Zero-Valent Pb by Cementation Using Zero-Valent Fe, Minerals 12 (2022) 723. https://doi.org/10.3390/min12060723.
[63] L.R. Pederson, Two-dimensional chemical-state plot for lead using XPS, J. Electron Spectrosc. Relat. Phenom. 28 (1982) 203–209. https://doi.org/10.1016/0368-2048(82)85043-3.